MASTER THESIS

Capacitive Micromachined

Ultrasonic Transducers

Vidar Forsmo

Horten, YEAR 2007

Submitted to the Faculty of Science and Engineering, Vestfold University College, in partial fulfilment of the requirements for the degree Master of Microsystem Technology.

Abstract

Ultrasound technology is a powerful tool in medical diagnosis. While piezoelectric ultrasonic transducers are dominant on the marked at present, capacitive transducers-cMUT- are being explored as a complementary technology. The cMUT is a device produced by silicon surface micromachining technology and can compete on production cost and other technical aspects. This thesis presents the design of a single element cMUT transducer, and it is shown how the design can be extended to an array. The fabrication processes is suggested. The motivation for choosing the different process steps is partly based on methods developed at NTNU [1] and make new processes to fit the same frame of work. Some of the process steps are new and not tested in this concept. The techniques are however well known from other MEMS-applications.

The first steps of analytic and numeric models are made up to describe the behavior of the transducer. The results for the mechanical modeling are consistent and give confidence to the models. It is shown how an equivalent circuit can describe the lumped model of the cMUT.

The suggested method of fabrication is prepared by making a mask layout in L-Edit software.

Table of contents

1   Introduction

The report will deal with a relatively new technology of making ultrasound transducers. Piezoelectric transducers are the commercial devices of today. The upcoming of new or the maturing of existing processing techniques encourage the scientific community to look for alternative ways of realizing the same functionality. It is also often the end user asking for a device with specific of special functionality. These demands may not be met by traditional technology.

This report is a part of a major project started at Vestfold University College (HVE). This is a project in collaboration with Rikshospitalet University Hospital in Oslo. They wanted a small inexpensive ultrasound transducer for heart monitoring during and after major surgery.

The purpose of this report is to make an initial design of an ultrasound transducer based on electrostatic forces. The cMUT (Capacitive Micromachined Ultrasonic Transducer) is using electrostatics to operate the device. The problem consists of designing and modeling a single element transducer. The cMUT is to be described by both analytical and numerical models. A proposal on the fabrication processes is included. The aim is to design a cMUT operating at 10 MHz, with element dimensions not exceeding 2 mm in diameter. Included is also to show how to contact the surrounding electronics. It is however out of the scope of this work to look into the electronics. Also, the packaging of the transducer is to be handled in other projects.

The contents of the work is first to describe the principles of ultrasound transducer. Comparing the cMUT technology to the traditional technology is important to better se if the advantage of introducing new technology is substantial. Next step is to give a complete description of a likely fabrication process. The emphasis is on suggesting processes which is possible to realize in practice. A cMUT has to be modeled for the specifications given in the problem. Analytical modeling is done to get an understanding of the behavior of the cMUT. To get confirmation of the results and additional information, numeric modeling has to be done. The modeling will also give the specific dimensions of the structure. When all the structural dimensions are fixed and the process parameters are in order, the necessary mask layout for the lithography is made.

The model presented here is for a 10 MHz, 2 mm diameter single-element or annular array transducer. The models and calculations are available as Mathematica 5.2, Comsol Multiphysics 3.3 and L-Edit v12.1, and simple parameter changes in these files should allow the design to b easily modified to other diameter and frequency combinations.

2   Ultrasound measurement system

Ultrasound measurement system is a system for examining an object without taking it apart or operating on it. This system is based on sound waves and the reflection of these. The idea is to send sound waves in to an object. The waves will reflect or scatter when encountering barriers or inhomogenities in the object. The reflections will reach the measurement probe with different time delays. As the speed of sound is known, these delays can be interpreted as distance and presented as an image. Ultrasound is defined as sound waves over the audible rage. The audible range is from about 20 Hz to 20 kHz. A high frequency allows a short pulse and narrow beam, hence, good image resolution. However, the attenuation increases with increasing frequency. Most ultrasound waves used for medical purposes are in the range fro 2-10 MHz. In special cases frequencies up to 40 MHz can be used [2]. The connection between frequency and wavelength is:

$$\lambda = \frac{c}{f}$$
(1)

The wavelength λ is inverse proportional with the frequency f . c is the speed of sound in the medium to be probed. This simple equation describes the trade off in use of ultrasonic transducers. The attenuation of waves will increase with shorter wave lengths. A high frequency transducer will have a wave propagation suffering from attenuation and will not be able to penetrate deep in to the object to be examined. On the other hand, the resolution of the transducer will increase with higher frequencies. It is obvious that this trade off is very important in the design of a transducer using sound wave propagation. Ultrasound measurement systems have a wide variety of applications. Depending on the use, different frequencies and intensities are implemented. It is used in industrial as well as medical applications. When used for testing or examination the common denominator is the non destructive nature of the transducer. In the industry is possible to test mechanical, e.g. metallic, structures for flaws. For metals high frequencies are used, as they are homogeneous and do not attenuate ultrasound. It is possible to examine most materials. Lower frequencies are used for more inhomogeneous materials giving high attenuation, such as concrete and wood. Today many production facilities have ultrasonic equipment placed for in situ testing of the products.

The noninvasive character of the ultrasound testing is well suited for use on humans. Most people are familiar with the use of ultrasound to monitor the fetus in the mother's uterus.

Ultrasound is also used for cardiac monitoring, detection of tumors, measuring blood flow and investigating other internal organs of the body.

The ultrasound measurement system consists of several parts. The ultrasonic transducer is a small but very important part of the system, as it has the task of sending and receiving the acoustic signal. Electronics provide the signal manipulation and interpretation. The transducer may be a single element that is moved to form an image, but today it is more common to use an array that can be controlled electronically to scan in different directions to obtain an image. Finally the computed signal is viewed in a screen which provides the final images. The objective for this project is to design a new transducer. The intention is that the transducer is compatible with existing ultrasound technology for signal processing.

3   Technology of Ultrasonic Transducers

The traditional ultrasound transducer is based on piezoelectric materials, mostly PZT. This is a mature technology with well designed applications which has been on the marked for over 30 years. The ability of a piezoelectric material to change form is also utilized in other fields of science. By applying a voltage over a piezoelectric material it will contract or expand according to the polarity of the voltage. An AC will induce a pulsating motion being able to emit ultrasonic waves. The reflected wave will be detected in the opposite way; the sound wave will make the material change shape and induce a voltage to be measured.
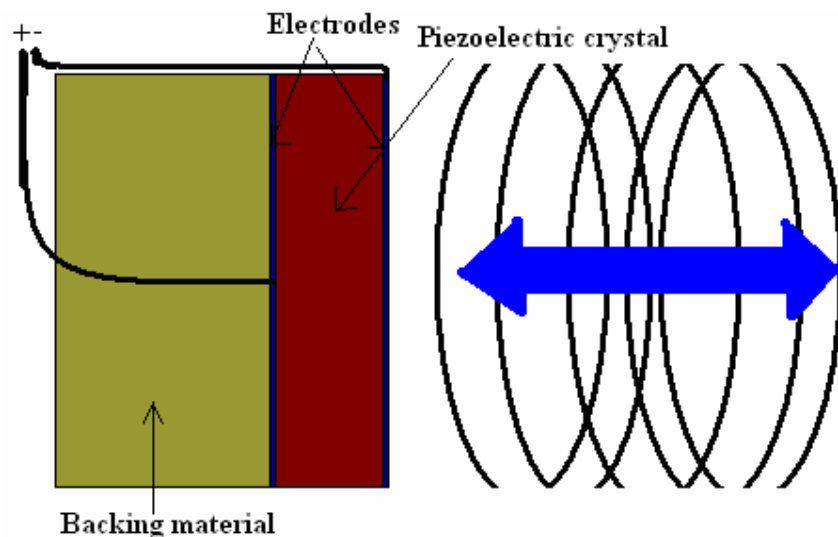

Figure 3.1 Principle of piezoelectric transducer

In recent years a new technology of ultrasound technology has emerged. It is an electrostatic transducer made by surface micromachining. A cMUT is build up by many drum-like features on top of a silicon substrate.
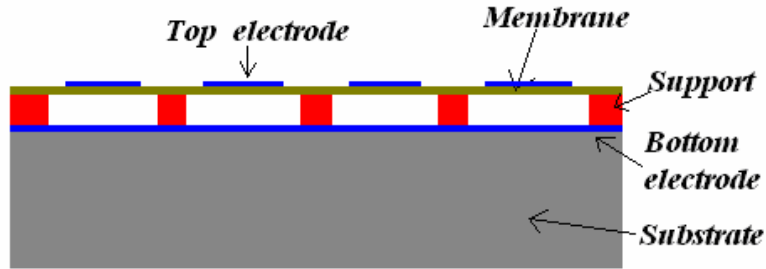
Figure 3.2 cMUT cells

The principles of a cMUT use the electrostatic forces over a small gap between two electrodes. Setting an alternating voltage over these electrodes, the electromotive force will force the membrane to deflect. The membrane motion will cause an oscillating pressure and hence, emit an ultrasonic wave. After a short transmitting sequence, the cMUT drum is ready to wait for the reflection. The reflected wave hits the membrane, and causes the membrane to vibrate. The change in distance between membrane and substrate will give a capacitive change between the electrodes. The change in capacitance is the basis for building up the ultrasonic picture. There are several research groups working on the different challenges of the cMUT. Still the technology is not commercially available but the feasibility of cMUT transducers has been demonstrated in several ultrasound applications [3, 4].

3.1   Differences between piezoelectric and cMUT technology

There are different arguments for looking at alternative technologies in the ultrasound transducer. Today the traditional transducers functions very well but most piezoelectric transducers are based on dimensions of $1/2\lambda$. They are working on resonance frequency to get the best efficiency. When making high frequency transducers, the wavelength becomes increasingly smaller and the demands for precision on the production line increases. As a consequence the cost rises. By using cost effective silicon micromachining, based on IC-technology, surface micromachined transducers may be produced at considerably lower cost. The cost reduction is due to the fact that the cMUT can be processed in large numbers on wafer level with existing technology.

Sound waves are heavily attenuated in the human body. To get a detectable reflected signal, the emitting burst is quite powerful, with pressure amplitudes of typically a

few Megapascals. One important aspect about the transducer is the transducer impedance. It is important to be able to mach the impedance to have best possible energy conversion form the transducer to the probed media. Acoustic impedance is the relationship between the density and sound velocity in a material [2].

$$Z_a = \rho c \qquad (2)$$

The acoustic impedance for some materials is:

Table 3.1 Acoustic impedance

Material	$Z_a \ (kg/m^2 s)$
PZT (piezoelectric material)	33.7×10^6
Air	400
Water	1.5×10^6
Aluminum	18×10^6

For probing in air the impedance matching for the piezoelectric transducer is becoming difficult. The difference in water and human body is not that large. The difference can be compensated for with impedance matched layers between the media and transducer. The importance of getting a good impedance match is evident in the ring down time of the transducer. If the acoustic impedance of the transducer is higher than the media the transducer will not be damped and will continue to vibrate for a while after the signal is turn off. The ring down occurs because of the resonance frequency operation of the transducer. This will result in a longer pulse, hence, lower axial resolution for the system. One of the benefits of the cMUT is the possibility for high bandwidth operation and thereby a short pulse time. The specifications for a piezoelectric crystal are set when fabricated and cannot be altered. As shown in chapter 6, small adjustments on important parameters can be done on a cMUT transducer. This is due to the necessary biasing of the capacitor. It enables some tuning of the transducer, which can show to be useful.

Often it is a desire to make several parts of a system on the same base. Integrating features in the same system is in most cases beneficial and cost effective. The cMUT is a surface micromachined device made on top of a silicon substrate which makes integration with electronic parts of the system possible.

The upcoming of new technology in the field of ultrasound transducer is basically a widening of the use of ultrasound. Even if the cMUT technology has promising

aspects, it will probably not replace existing piezoelectric technology in the foreseeable future. The different technologies are probably going to compliment each other. cMUT will probably first find its use in niche applications requiring e.g. low production cost, small size or easy integration with front-end electronics.

4 Fabrication of cMUT

The fabrication of a cMUT has been described by several authors [5], [6], [1]. There are several alternative ways to produce a working cMUT. The main principle of actuating the ultrasound and capacitive sensing of the reflected wave is basically the same. Most of the techniques are familiar micromachining methods with pros and cons. The most used fabrication method is to use sacrificial layers to form the cavity between the two electrodes. This method implies a several process steps including mask layout and photolithography. The removal of a sacrificial layer also includes the challenge of avoiding stiction in the process. Reducing the number of step will also reduce the production cost of the transducer.

4.1 Description of the fabrication process

There has also been work done with processes not including the removal of a sacrificial layer. Both Huang et al. [7] and recent work by Midtbø [1] shows a fabrication method preparing the membrane and substrate separately, bonding them together without having the issue of removing a sacrificial layer. In order to give a simple production process and cooperative work with the researchers at NTNU and Sintef, the fabrication method used in this paper is based on the fusion bonding technique described in [1].

4.1.1 Bottom substrate with bottom electrode

The base of the transducer is the silicon substrate. In order to get the gap between top and bottom electrode as close as possible, it is imperative to get the bottom electrode on top of the substrate.

Figure 4.1 Doping to get bottom electrode

The test-process described by [1] assumes the bottom electrode placed beneath the substrate. This reduces the sensitivity and requires high voltage to actuate the transducer. To improve the sensitivity and lower the actuating voltage, the electrode must be placed on top of the substrate. Two alternative bottom leads can be

considered used on top of the substrate. The most beneficial alternative in an electrical point of view is metallization leads, as this minimizes resistance. However, depositing a metallization layer on top of the wafer results in a topographical problem. The need for a smooth wafer surface is essential for the bonding process. An alternative is doped leads inside the substrate. This will open for the possibility of fusion bonding. Both diffusion and implantation are doping methods possible. Using implantation, it is uncertain if the wafer surface of will stay smooth enough after annealing. The probability of roughening the surface, introduce the need for masking the wafer and pattering the doped leads in order to minimize the lead area concurring with the fusion bonding area. Heavy doping of the substrate can also be achieved by diffusion. Diffusion is assumed not to influence the surface properties of the wafer and allows doping of the whole wafer area. Diffusion–doped substrate has not been tested for this application, and changes in bonding strength have to be further investigated. Uniform doping of the substrate will lower the resistance and one mask layer is spared. Doping a n-type substrate (100) with 4-h phosphorous gas phase drive in at 1000˚C, a sheet resistance of less than $1.5\,\Omega/\square$ can be achieved. The use of doped silicon as bottom electrode is described in [8], [9].

4.1.2 Nitride deposition on top substrate

The purpose of the top substrate is to temporarily support the membrane until it is fused to the wafer. First step is to cover the wafer with Si_3N_4. The deposition is done by low pressure chemical vapor deposition (LPCVD).

Figure 4.2 Depositing top wafer with silicon nitride

The process can be tailored to produce layers with different properties. Low residual stress is an important factor in the production of good cMUT membranes. The residual stress is plotted in figure 4.3 [10] as a function of gas ratio and temperature. By altering the ratio of SiH_2Cl_2 and NH_3-gas, the residual stress even can be

compressive. The process is very dependent on the process temperature. It is beneficial to use high temperatures to produce a low stress membrane.
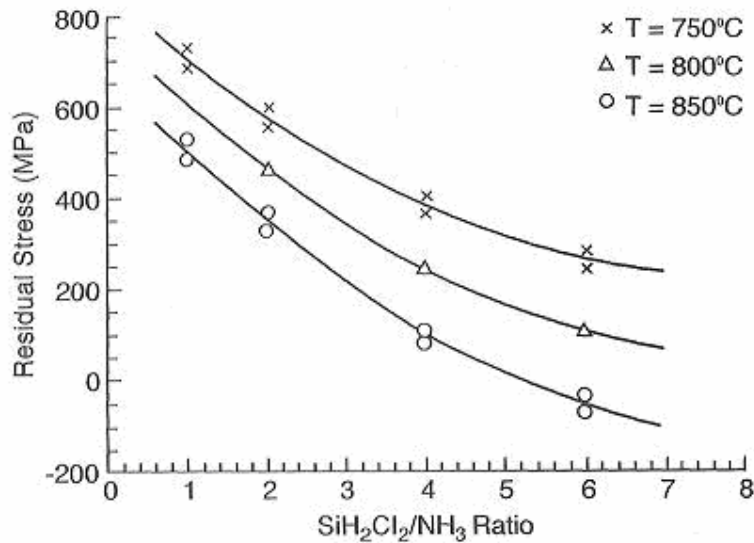

Figure 4.3 Residual stress vs. gas composition and temperature from [10]

The nitride properties are altered depending on the gas ratio and temperature. There are practical limitations giving some residual stress in the produced membrane. Residual stress as low as 80 MPa is reported [11]. Conventional film depositing methods typically gives residual stresses of several hundred MPa. Increasing residual stress results in a stiffer membrane. A stiffer membrane demands higher power consumption, and is not desirable in most applications. The thickness of the nitride layer is equal to the sum of the membrane thickness and the height of the support walls of the cell. With a gap height of 200 nm and a membrane thickness of 200 nm the nitride layer deposited must be 400 nm.

4.1.3 Cavity definition

The cavity of the cMUT is defined in the nitride layer. This part of de design has not been documented or tested and introduces a new aspect to the cMUT design. By choosing to define the cavities in the nitride layer, it is possible to get the bottom electrode up on top of the substrate. In order to get a well defined cavity with good control of the dept, reactive ion etch, RIE, is the preferred method. Sintef delivers a process with in situ laser depth control of the RIE process.
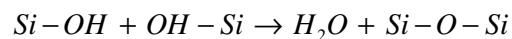
Figure 4.4 RIE etch of the cavities

The repeatability of the process is estimated at ±1% deviation on wafer level. The high quality definition of the cavity introduces an advantage to the method of using sacrificial layer. Using sacrificial layer to define the cavity the membrane has to be pierced from the top side and the release etch is done trough these holes. The release etch is isotropic and the lateral dimensions of the cavity is defined by the positions of the trough holes and time control. The release etch procedure also has to include actions to avoid stiction.

4.1.4   Hydrophilic Fusion Bonding

The two wafers must be cleaned and rinsed thoroughly to get a smooth and clean surface for the bonding process. The preparations are described in [1], giving the details of the process. In order to enhance the bond strength, the nitride wafer is oxidized. The best result proved to be the plasma oxidation. The bond annealing is done in 1050˚C for 2 hours. The hydrophilic fusion bonding is thought to happen by a polymerization of silanol.

$$Si-OH + OH-Si \rightarrow H_2O + Si-O-Si$$

The plasma oxidations give a higher concentration of –OH groups and thereby give higher bond strength as a result.
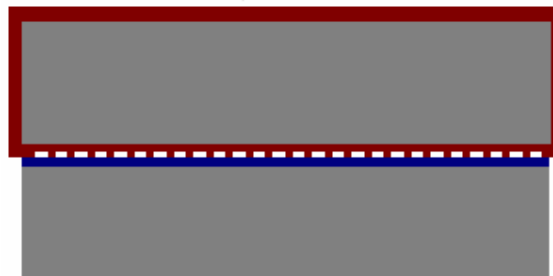

Figure 4.5 Fusion bonding

4.1.5 Etching the top wafer

When the bonding process is competed, there is no need for the wafer supporting the nitride layer. The whole top wafer is to be etched away. To keep the bottom wafer out of harms way, it is covered by a 750 nm layer of SiO_2. The nitride is opened up by dry etch using the silicon as the etch stop in the process. This allows access to the top silicon wafer. The wafer is removed by TMAH at 80˚C. The thick oxide layer covering the bottom wafer protects it in this process. The side poles of the nitride are just broken away in the process. This will not include an additional working step. The use of the protective oxide layer is over and is removed by BuHF. The result is a silicon wafer covered with membranes of silicon nitride.
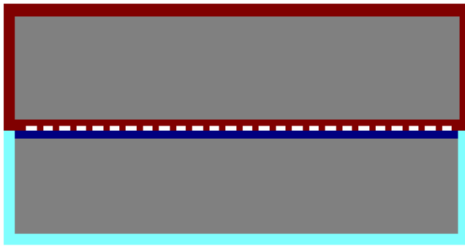
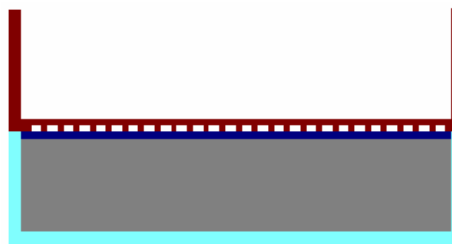**Figure 4.6 Oxidizing the bottom wafer**   **Figure 4.7 Etching the top wafer**

Figure 4.8 One wafer packed with cells

4.1.6 Top electrodes and contact pads

After bonding and subsequent wafer etching, the whole support wafer is covered by Si_3N_4. Both electrodes of the transducer must be accessed from the top side. The nitride covering the designated contact pad area must be removed, including a separate masker layer and etching step.

Figure 4.9 Etching access to the bottom electrode

The second electrode made of aluminum, is sputtered on top of the membrane. Sputtering is recommended deposition method to maximize the step coverage of the element. In contrary to the bottom electrode, the top electrode must be patterned to match each cell. In designing the electrodes, some considerations have to be made; there is a trade of between low mechanical influence of the electrode and low electrical resistance. The optimal electrode area is half of the cell area. Interconnections should be 3 µm wide and the thickness of the aluminum layer should be 200 nm [12].
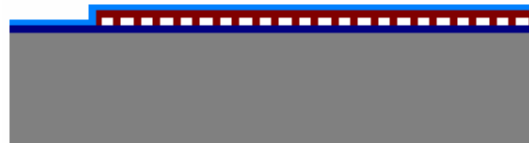
Figure 4.10 Sputtering of top electrode

The metal depositions must be carried out in two separate operations. The thickness of 200 nm is to thin for the contact pads on the element. Bonding connecting wire to a pad with that thickness is not recommendable. Depositing aluminum is done by sputtering the whole wafer and defining by lithography the areas to etch off. The first operation is to set the thick areas of contact pads. When having to use an extra mask to do this operation, adding thickness to the leads going outside the cMUT-element is convenient to include.

4.2 Fill factor

In the piezoelectric transducer the entire surface of the transducer is moving and thereby creating an effective emitting and receiving surface area. In a cMUT transducer the transmitting and emitting surface consists of many individual cells. The cells have to be supported and the support structures create a "dead" area on the surface. In transmitting mode the dead area is reducing the power of the ultrasound wave. It is important to decrease the inactive area of the transducer. Two main considerations can be made to deal with the problem. The cells have to be as close as possible to each other. The limit is how thin the support walls can be constructed. It can both be a process limitation and an adherence problem, i.e. to obtain sufficient adherence of the membrane to the substrate. Second, the design of the individual cells influence how well they fit to each other. Several published designs[9, 11] are based on a hexagonal structure of the cell. This pattern gives a high packing density. The hexagonal cell is however more difficult to model and the behavior must be examined in numerical analysis. A circular membrane is easier modeled and can give fairly consistent results from both analytical and numerical analysis. It is also common in the literature to use a hexagonal layout, but model the cell as a circular with an effective radius. This work uses a circular cell with layout shown in figure 4.11.
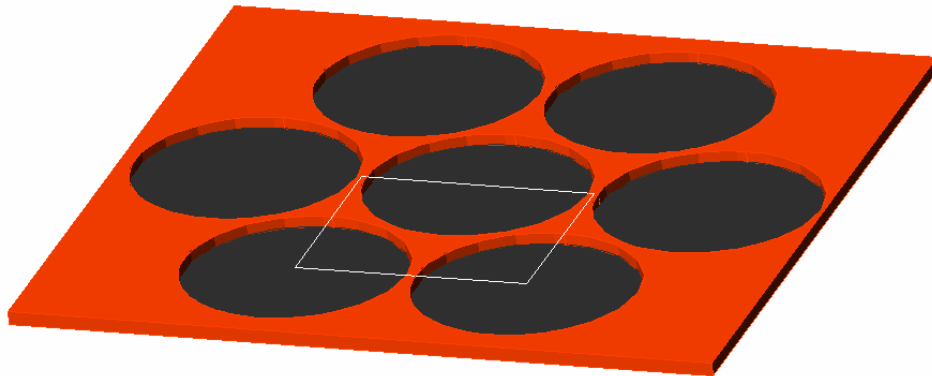

Figure 4.11 Circular element structures

The thin marked square indicates the unit cell of the element. The unit cell consists of one full cell (one half and two quarters) of active area. The rest of the unit cell is support area. In a design with cell radius of 10 µm and 20.8 µm pitch the fill factor is;

$$\frac{\pi r^2}{p^2 \operatorname{Sin}(60°)} = 0.84 \tag{3}$$

Where r is the radius and p is the pitch. If the cells were to be arranged in an annular fashion in stead of rows, the pitch in the radial direction increases from $p\,Sin(60^\circ)$ to p. The fill factor decreases to;

$$\frac{\pi r^2}{p^2} = 0.73 \qquad (4)$$

For a hexagonal cell structure the fill factor will improve. Like in the circular structure the unit cell consist of one full transducer cell.

Figure 4.12 Hexagonal element structures

The fill factor for the hexagonal cell structure is:

$$\frac{6r^2\,Tan(30^\circ)}{p^2\,Cos(30^\circ)} = 0.93 \qquad (5)$$

The pitch p of 20.8µm in the two structures is the same and the radius has the same numerical value but in the hexagonal cell it is the inner radius. The difference in fill factor is 9%. The significance of this difference is discussed in [13]. The comparison of hexagonal and circular membrane may be too simple. The use of wafer bonding technology opens the possibility of using other membrane formations like square or quadratic. Even membranes with masses can be utilized [14].

4.3   Packaging

The transducer, fabricated according to the previous chapters is not insulated. The top electrode is in the open. When the element is connected electrically, two wires will extend considerably above the surface of the transducer. Depositing a thin insulating layer of Si_3N_4 is therefore not sufficient. The insulating material may be the final package of the transducer. One suggestion is to use a silicone based package that can serve as both an insulator over the whole device and giving proper impedance matching properties. This package/insulator should be thin to avoid influencing on the range of the transducer. Designing the package is however out of the scope of this project.

5   Analytical modeling

The fabrication processes provide some of the parameters needed for the overall design. These parameters are needed for modeling the behavior of the transducer. When choosing materials for building the device, material specifications follow. A silicon nitride membrane has a specific Young's modulus, Poisson ratio and density. Also the level of intrinsic stress is a fabrication process variable. A good model of the transducer is needed for several reasons. First it will give valuable information already at the first theoretical levels. Second, a good model will reduce the cost of prototypes considerably. Alterations in a theoretical model are much less expensive than having to produce several prototypes. In order to be confident in the modeling results both analytical and numerical modeling is necessary.

5.1   Resonance frequency

cMUT transducers, like piezoelectric transducers, are operating on resonance frequency to get best possible ultrasound output, and high sensitivity in reception. The aim for this design is to come up with a transducer operating at 10 MHz. Using a Si_3N_4 membrane, intrinsic stress from fabrication can be a major factor in setting the operating frequency. The resonance frequency increases with increasing intrinsic stress. At low tress levels the membrane behaves as a plate with the material parameters giving the plates own stiffness and frequency. As intrinsic stress level increases, this stress will dominate over the flexural rigidity. The membrane will operate more as a membrane with no bending stiffness. The basic calculations of a circular membrane in ch. 5 is described in [15]. This reference gives the wave equation used for solving the plate resonance frequency as a fourth order partial differential equation;

$$\nabla^4 y + \frac{12\rho(1-v^2)}{Et_{mem}^2}\frac{\partial^2 y}{\partial^2 t} = 0 \tag{6}$$

Where y is the deflections, E is the Young's modulus of the membrane, v is the Poisson ratio, ρ is the density of the membrane and t_{mem} is the thickness of the membrane

Solving with boundary conditions no deflection and rigid fastening at the border;

y(a)=0 and $\left.\dfrac{dy}{dr}\right|_{r=a}=0$, gives the resonance frequency of the first mode as;

$$f_r = 0.47\frac{t_{mem}}{a^2}\sqrt{\frac{E}{\rho(1-v^2)}} \tag{7}$$

In the plate model intrinsic stress is not considered. It is only material dimensions and properties which determine the resonance frequency. For a transducer with radius of 10μm and thickness of 200 nm the resonant frequency for this model is 9.638 MHz. For comparison, a logarithmic plot in figure 5.1, the resonant frequency of the membrane is plotted as a constant.

The silicon nitride membrane is most often manufactured with intrinsic stress. A model for an oscillating membrane, neglecting bending forces, can be found in several textbooks, e.g.[15] The equation of motion for this membrane is a second order wave equation

$$\nabla^2 y - \frac{1}{c^2}\frac{\partial^2 y}{\partial t^2} = 0 \qquad \text{with} \quad \frac{1}{c^2} = \frac{T}{\rho} \tag{8}$$

Solving for a circular membrane in polar coordinates, gives a solution with Bessel functions. The interesting mode for a cMUT transducer is the first mode. The resonance frequency for this mode is.

$$f_r = 2.4048\frac{1}{2\pi a}\sqrt{\frac{T}{\rho}} \tag{9}$$

As the solution indicates, the resonance frequency has a quadratic dependency on the intrinsic stress. The solution is given in a logarithmic plot in Figure 5.1

The two solutions are combined in figure 5.1 and illustrate the point where intrinsic stress will dominate the stiffness of the membrane. Near the crossing point at 207 MPa, it is expected to find a transition area were both solutions influence on the resonance frequency.
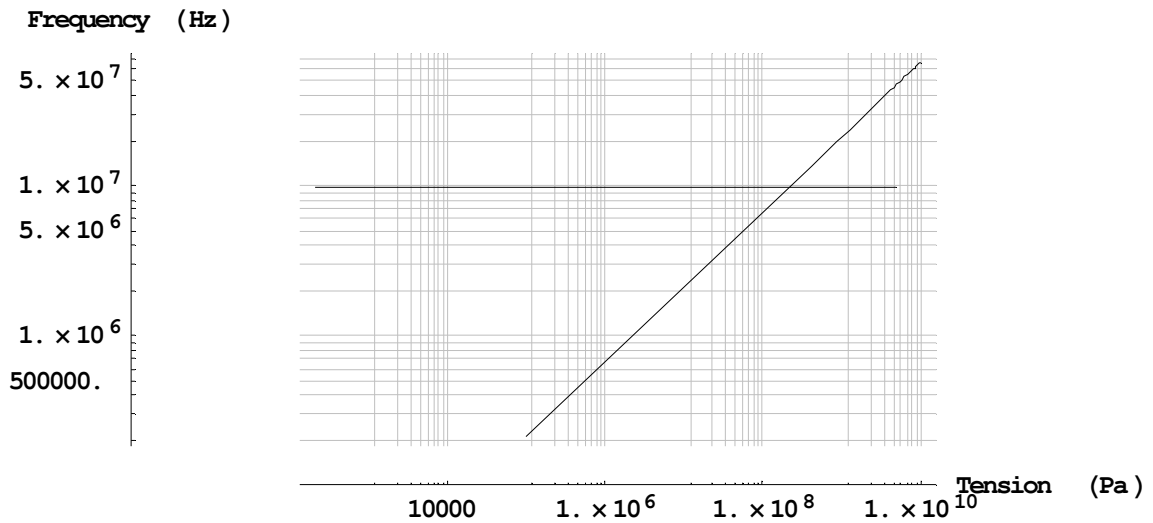
Figure 5.1 Combined plots of resonance frequencies

A single solution for the resonance frequency, taking both plate and membrane theory into consideration is not found in the literature. Such a solution is complex and is not done for this project. The two asymptotic solutions plotted in Figure 5.1 give us valuable information. As referred to in the chapter on fabrication, the intrinsic stress can be tuned in the deposition process. In production of the transducer, stress variations between batches and even in different positions on one boat occur. To ensure production of transducers with equal performance, control of the intrinsic stress is important.

Setting the stress level well below 208 MPa should make it possible to get the intrinsic stress out of the equation. The transition region is discussed further in the numerical modeling part of the report. From the results on resonance frequency, the material parameters are determined. They assume deposition method giving low stress membrane, setting membrane stiffness as dominating property.

Table 5.1 Transducer properties

Young's modulus	320 GPa
Poisson ratio	0.263
Density	3270 kg/m³
Relative permittivity, ε_r (stoichiometry dependent)	7.5
Membrane radius, a	10 µm
Membrane thickness, $\mathbf{t_{mem}}$	0.2 µm
Gap membrane/substrate, t_{gap}	0.2 µm

5.2   Mass spring system- collapse voltage

The membrane of the cMUT can be described as a simple mass spring system.[11] By analyzing the forces acing on the mass, a simple understanding of the problem is available.

$$F_{capacitor} + F_{spring} = F_{mass}$$

There are two main forces acting when the membrane is deflected. The electrostatic force will pull the membrane down towards the bottom electrode. The stiffness of the membrane, represented by a restoring spring force will resist the electrostatic force. Both transmitting and receiving mode of the transducer is making use of these two forces. With use of principle of virtual work, the electrostatic force can be modeled as a plate capacitor. The electrostatic force is then:

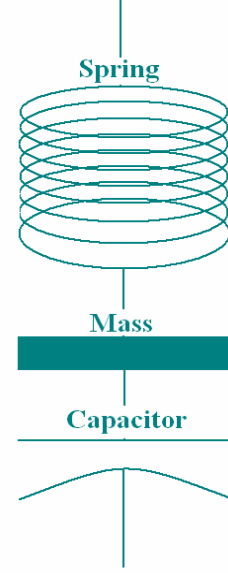$$F_{capasitor} = \frac{\varepsilon \varepsilon_0 A V^2}{2(d_0 - y)^2} \tag{10}$$

Figure 5.2 Mass spring relationship

Where F is the force, A is the plate area, d_0 is the original gap, y is the displacement, ε and ε_0 is the dielectric constant of the membrane and free space respectively. The force is not linearly dependent on the electrode gap distance. The restoring force on the membrane is the spring force, linearly dependent on movement x and the spring constant k.

$$F_{spring} = -ky \tag{11}$$

Increasing the voltage, the electrostatic force will dominate the spring force, resulting in a collapse of the membrane. The limit for membrane deflection before collapse can be calculated by introducing stable state [16] conditions;

$$\frac{dF}{dy} < 0 \Rightarrow \frac{A\varepsilon\varepsilon_0 V^2}{(d_0 - y)^3} - k < 0 \tag{12}$$

This requires:

$$y < d_0 / 3 \tag{13}$$

The collapse voltage is dependent on material and structural parameter like the spring constant k, area A and the original gap distance d_0.

$$V_{collapse} = \sqrt{\frac{8 k d_0^2}{27 \varepsilon \varepsilon_0 A}} \qquad (14)$$

For the cMUT with the electrode on top of the membrane, the gap distance d_0 is the sum of membrane thickness and vacuum gap. d_0 is 400 nm. The solution for the collapse voltage based on a parallel plate model. The electrostatic force is uniform trough out the area of the plate. For a cMUT the model is a simplification. The curved shape of a strained membrane has variable electrostatic force. The force decreases in an annular fashion moving away from the membrane center. Variable gap spacing has been modeled recently [17] but is not included in this work. The spring constant k can be derived from table 11.2 in [18] and can be expressed as;

$$k = \frac{64 E \pi t_{mem}^3}{3a^2 (1-v^2)(Ln4-5)} \qquad (15)$$

Where E is the Young's modulus t_{mem} is the membrane thickness. a and v are the membrane radius and the Poisson ratio respectively. Inserting membrane properties in equation for collapse voltage, the resulting voltage is 30.76 V. The voltage is expected to be lower than the real transducer because of the parallel plates giving a larger area closer to each other thereby creating higher electrostatic force. In [19] the collapse voltage is calculated with a metallization layer and incorporating the spring constant in the expression;

$$V_{collapse} = \gamma \sqrt{\frac{128(E-T)t_{mem}^3 d_0^3}{27\varepsilon_0 (1-v^2)a^4}} \qquad (16)$$

$\gamma = 0.82$ for half metallization. Assuming no tension T, the collapse voltage is 28.15V. Introducing intrinsic stress of 208 MPa the collapse voltage is 28.14V. In this case the stress has negligible effect on the performance.

5.3   Equivalent circuit of a cMUT

The cMUT can be modeled as a two port circuit in order to get a deeper understanding of how the transducer works. The circuit is divided in two parts. On the one side there is an electrical part describing the wiring and the different electrical impacts on the overall performance. The second part of the circuit is a purely mechanical system describing how the physical parameters influence the transducer. The standard way of describing the lumped model is taken from[11], originally due to Mason[20]. It is important to understand the connections in this two port system. For the design of the membrane it is necessary to have a good understanding of how the capacitive force is acting on the membrane.
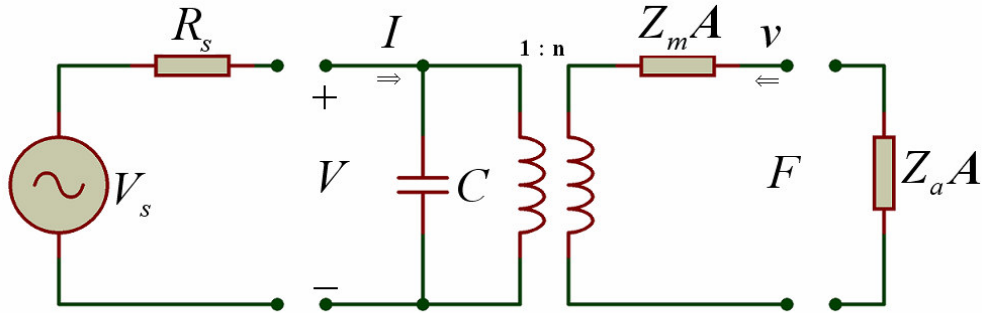

Figure 5.3 Equivalent circuit of a cMUT

Figure 5.3 illustrates the equivalent circuit for a cMUT. The left hand side is the electrical part whereas the right hand side is the mechanical part of the transducer. The electrical components are the power source, electrical resistance and the capacitance over the two electrodes. The transformer with turn ratio 1:n, models the coupling between the electric and acoustic part of the transducer. The mechanical side consists of both mechanical and acoustic impedance. Equivalent expressions are current $\Leftrightarrow$ flow and voltage $\Leftrightarrow$ force.

The displacement of a circular membrane is described in the differential equation [11].

$$\frac{(E-T)l_{mem}^3}{12(1-v^2)}\nabla^4 y(r) - l_{mem}T\nabla^2 y(r) - P - l_{mem}\rho\frac{d^2 y(r)}{dt^2} = 0 \qquad (17)$$

The solution assuming harmonic excitation the solution can be expressed in the form of mechanical impedance of the membrane.

$$Z_m = \frac{P}{v} = j\omega\rho t_{mem}[\frac{t_{mem}ak_1k_2(k_2J_0(k_1a)J_1(k_2a)+t_{mem}k_1J_1(k_1a)J_0(k_2a)}{ak_1k_2(k_2J_0(k_1a)J_1(k_2a)+k_1J_1(k_1a)J_0(k_2a)-2(k_1^2+k_2^2)J_1(k_1a)J_1(k_2a)}](18)$$

Where,

$$k_1 = \sqrt{\frac{\sqrt{d^2+4c\omega^2}-d}{2c}} \quad k_2 = j\sqrt{\frac{\sqrt{d^2+4c\omega^2}+d}{2c}} \quad c = \frac{(E-T)l_{mem}^2}{12(1-v^2)\rho} \quad d = \frac{T}{\rho} \tag{19}$$

Reference [11] contains a typographical error in its expression for parameter c, as the density ρ is missing. This is corrected in [9]. Since the cMUT transducers are operated by both a dc and an ac voltage. The electrostatic force depends on the applied voltage in second power. In a small signal model and assuming $V_{dc} \gg V_{ac}$ and $C_{ac} \ll C_0$, the current can be expressed as

$$I = \frac{d}{dt}Q = C_0\frac{d}{dt}V_{ac}(t) + V_{dc}\frac{d}{dt}C_{ac}(t) \tag{20}$$

By differentiating the C_{ac}, we get;

$$\frac{d}{dt}C_\alpha(t) = -\frac{\varepsilon_0\varepsilon^2 A}{(\varepsilon_0 l_{mem}+\varepsilon d_g)^2}\frac{d}{dt}d_g(t) \tag{21}$$

Were d_g is the vacuum gap. The derivative of the gap distance d_g is the membrane velocity and the coupling factor becomes:

$$n = V_{DC}\frac{\varepsilon_0\varepsilon^2 A}{(\varepsilon_0 t_{mem}+\varepsilon d_g)^2} \tag{22}$$

The result is current as a sum of electrical and mechanical components.

$$I = C_0\frac{d}{dt}V_{ac}(t) - n\bar{v} \tag{23}$$

In water the acoustic impedance is mush larger than the mechanical impedance. The equivalent resistance is

$$R_{eq} = \frac{Z_a S}{n^2} = Z_a\frac{(\varepsilon_0 t_{mem}+\varepsilon d_g)^4}{V_{dc}^2\varepsilon_0^2\varepsilon^4 A} \tag{24}$$

And the Q-factor of the transducer:

$$Q = \omega R_{eq} C = \frac{\omega Z_a (\varepsilon_0 t_{mem} + \varepsilon d_g)^3}{V_{dc}^2 \varepsilon_0 \varepsilon^3} \tag{25}$$

A variation in the bias voltage will influence on the Q-factor. For a cMUT, a large bandwidth is wanted and it is beneficial to aim for a low Q-factor. As mentioned in chapter 3.1 the pulse time and bandwidth relationship is $T_p = \dfrac{1}{B_w}$. By getting a large bandwidth the pulse time is reduced and the resolution increases. One drawback of the piezoelectric transducers is the inability to alter the mechanical properties after fabrication. From the above it is shown that the coupling factor and Q-factor can be adjusted by the bias voltage.

5.4   Electrical resistance in top electrode

For the design of the whole transducer it is important keep the losses to a minimum. While the electrical resistance in the bottom electrode is mentioned in chapter 4 to be as low as $1.5\,\Omega/\square$, the resistance in the top electrode is more dependent on the design of the transducer and the element. The top electrode consists of sputtered aluminum. Outside the element area the aluminum is 1, 2 µm and is not a source of any electrical loss. In the 4-element array layout of Ch 7.4 the maximal resistivity is in the lead to the center element. The resistivity ρ, of aluminum is $2.82\times10^{-8}\,\Omega m$. The lead is ≈ 550 µm long and 20 µm wide. This gives a maximum resistance in the leads of approximately 0.7 Ω. In the element itself, the resistivity is not straight forward to calculate. The hexagonal pattern of leads is spreading in all directions on the element surface. Assuming negligible resistance in the pad area, the resistance is in the leads connecting the cells. It is possible to build up a model for nodes in a hexagonal pattern in order to get an exact value of the electrical resistance. This is not done in this project. In order the get a very rough estimate of the resistance, the following method is used; A worst case scenario is

electrical connection only through one string of nodes with attached with leads to neighboring nodes. Figure 5.7 illustrates the current path for one node to the other. The element consists of 96 nodes across. The sheet resistance of the leads is;. All leads are 7µm long and 3 µm wide, resistance of one lead is 0.33 Ω. The resistance between the two adjacent nodes is seen from Fig. 5.4

$$\frac{1}{\dfrac{1}{0.33}+\dfrac{1}{2\times0.33}+\dfrac{1}{2\times0.33}}=0.17\Omega$$

Over the diameter of the element, the resistivity ads up to

Figure 5.4 Current trough top electrode

16.3 Ω. This value is too high and really not realistic Looking at the design in chapter 7 the contact pad is connected to 20 rows of cells. 20 rows are just $\frac{1}{5}$ of the width of the element. The resistance through 20 rows is less than 0.8 Ω. To get an accurate value of the resistance a suitable model should be presented. However, these rough worst-case estimates indicate that the top electrode resistance is small enough to ignore.
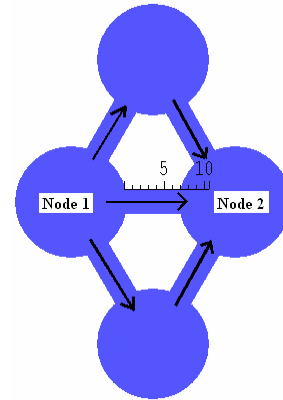
6   Numerical modeling

The analytical modeling of the problem is giving solutions which can be controlled for correctness. Analytical models are often over-simplifications of the original problem and therefore cannot give a completely correct answer. But they provide invaluable insight into the basic mechanisms of the problem, and how the different parameters play together to influence the result. In addition to the analytical modeling, a numerical model will help to complete the picture of the problem. A good numerical model solves the problem without having to set the limiting boundary conditions. The solutions coming from the numerical models are not easy to interpret and control and any wrong input will result in wrong output. The combination of numerical and analytical modeling is preferred.

For this project two different software for numerical calculations were available; Ansys (ANSYS, Inc., Canonsburg, PA, USA) and Comsol Multiphysics (COMSOL AB, Stockholm, Sweden). Comsol Multiphysics was chosen for the possibilities in the software to calculate with infinite boundaries, which is needed for emitting ultrasound into water.

6.1   Comsol Multiphysics modeling

The design for the transducer is a model with circular membrane. In numerical analysis any circular models can be evaluated as an axis symmetric 2D model. The model is made only by defining dimensions in two axes and making it all symmetric about z-axis. In this way the need for computer power is greatly reduced. The material parameters are explained in the chapter of fabrication. The dimensions of the transducer are based on the estimates from the analytic model.

Figure 6.1 Block build up of transducer

The model is drawn with a membrane radius of 10 µm and thickness of 0.2 µm. No other geometric features are included in the first model. The membrane is set to be symmetric about the z-axis on the left and is fixed on the right hand side. This will give a realistic comparison with the analytic model. The model will be expanded along with confident results.

6.1.1 Meshing of the model

In a numerical analysis the member to be analyzed is meshed into many elements. All
the elements are connected in nodes. To ensure proper meshing is used in the model,
several runs must be done with finer mesh in every run. In a numerical analysis it is
important to ensure that the number of elements, calculation points, is high enough to
give reliable output. However, setting the mesh to fine, the calculation will demand
much of the computer and make the calculations unnecessary slow without giving
more accurate results. It is important to set the meshing right. For the simple model in
chapter 6.2 the analysis were done in several runs with refining mesh in each run.

Table 2 Test results for refined mesh

Nr. of elements in z-direction	Frequency result (MHz)	Result change
2	9.623728	
4	9.619621	0.043%
8	9.618496	0.012%
16	9.618113	0.004%
32	9.617974	0.0015%

The refining mesh runs converged already at four elements on the height of the
membrane. A change in the result of 0, 043% is small compared to accuracy in
defining the dimensions of the membrane. Figure 6.2 illustrates the mesh in four
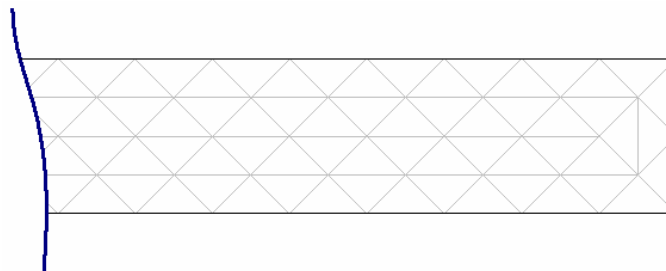element height.

Figure 6.2 Membrane mesh

6.1.2 Resonance frequency in clamped membrane

The resonance frequency is an important parameter of the transducer design. The task of the project is to design a transducer operating at 10 MHz. A cMUT is operating at resonance frequency, giving a concrete goal for the resonance frequency simulations. The solutions from analytical and numerical simulations results in setting the final physical dimensions of the transducer.

The first membrane model is suited to investigate the resonance frequency of the system and is comparable with the structure from the analytical calculation. The constraints for the membrane are set to free for all boundaries except at the clamped edge. This boundary is fixed so the simulation will not be able to calculate any transition areas around this area of the membrane. It is this kind of simplifications the analytical calculations are dependent on. The resonance frequency without any intrinsic stress is 9.62 MHz. This is the first mode frequency, which is the mode the transducer is going to operate in. In first mode all parts of the membrane moves in the same direction. Figure 6.3 illustrates the first mode at first resonance frequency of 9.62 MHz.
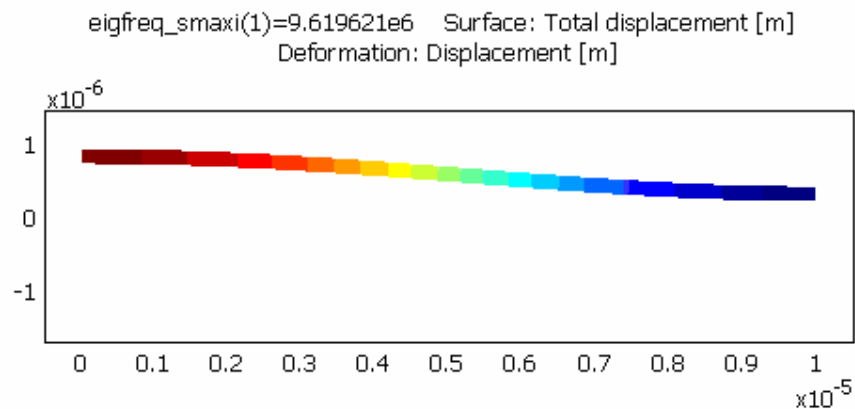

Figure 6.3 First mode

The analytic solution for the same problem was 9.638 MHz. This model has much of the same boundary conditions and it was not expected to be large difference between the two solutions. The difference is merely 0.2%. The match is considered excellent.

6.1.3 Contact pad

The aluminum contact pad is covering half of the membrane area and is stipulated to be made in the same thickness as the membrane. It will influence on the simulation result. The leads coming in to the pad is however not included in the calculation. The leads will ad to the stiffness of the system and may increase the resonance frequency somewhat.
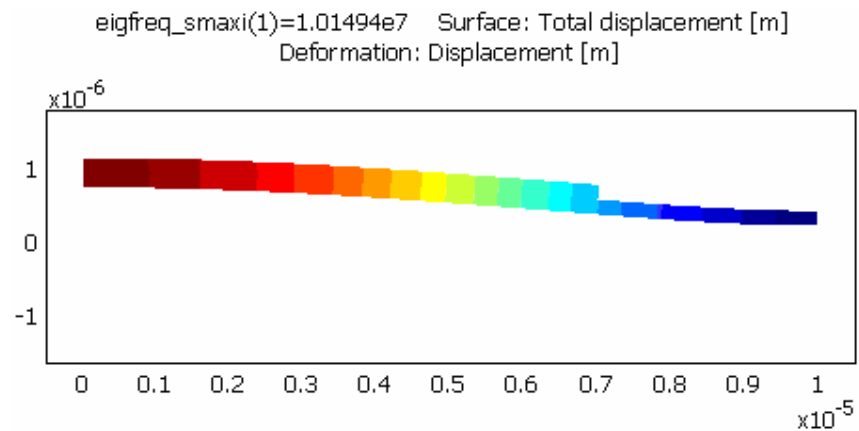

Figure 6.4 Resonance frequency with contact pad

With the same boundary conditions and meshing the alterations has, as expected, made the membrane stiffer. The resonance frequency has increased to 10.15 MHz, i.e. by 0.51 MHz.

6.1.4 The complete model

The advantage of a numerical model is among others, the ability to calculate the transition area where the membrane is attached to the support. The net step in the model is to introduce the support structure and the substrate. Figure 6.6 is the full model of the transducer. It also consists of a defined air gap of 200 nm between the substrate and membrane. The membrane is not rigidly fixed but connected to the nitride support. The fixed boundaries in the structure are the whole silicon substrate and the outer edge of the support, SiN2 and SiN3.

Figure 6.5 Layout of complete axis-symmetric model

Simulating for the resonance frequency resulted in a decrease compared with the previous model. The result was 9.93 MHz. The physical dimensions set in chapter 5 are relevant also to the numerical modeling.

6.1.5 Intrinsic stress

The preceding simulations are done with no intrinsic stress included in the model. In the analytical modeling, intrinsic stress proved to be an important parameter in the final design of a cMUT with Si_3N_4-membrane. In Comsol Multiphysics, initial stress is applied on subdomain level. In the simulations increasing stress levels are added and the frequency response is noted.
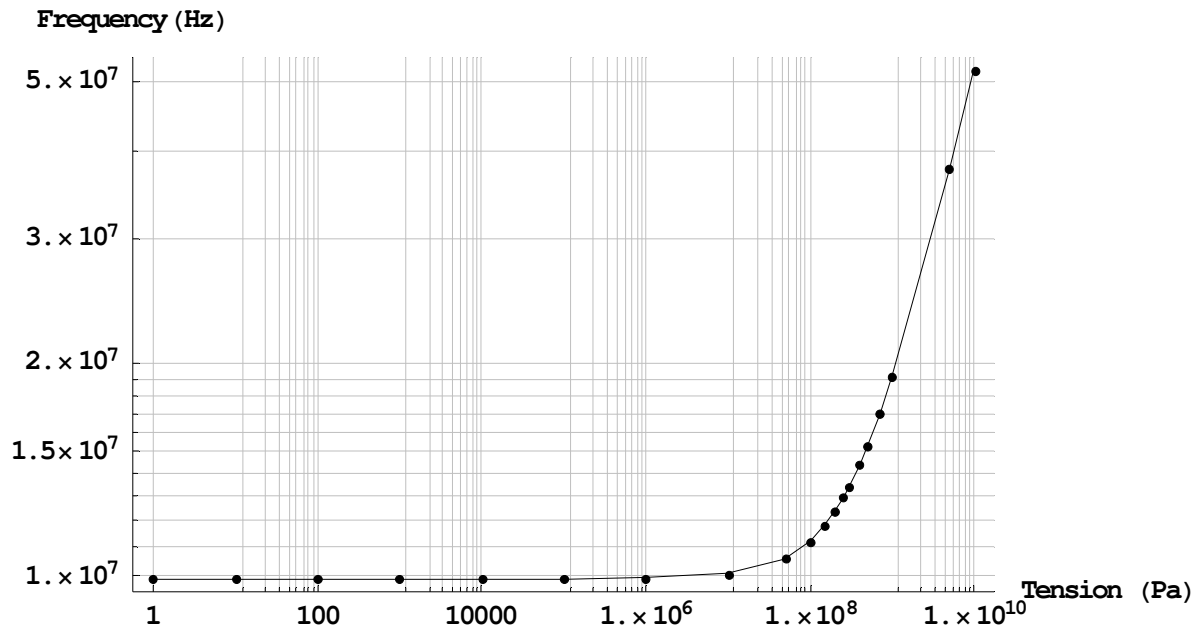

Figure 6.6 Resonance frequencies vs. intrinsic stress

The plate vs. membrane issue discussed in ch. 5 is evident also in the Comsol Multiphysics model. Without having any tensile stress in the nitride membrane, the resonance frequency is 9.93 MHz. The frequency does not change significantly until the stress is in the region of 50 MPa. From 50 to about 200 MPa the results indicate a transition face. This is expected from the analytical results. It is in this region the tension in the membrane starts to dominate over the material stiffness. The plot in figure 6.6 is a result of 18 separate simulations. The values giving the base for the plot is tabulated in appendix 1.

6.1.6 Analytical and numerical modeling of resonance frequency

Combining the result for both the analytic and numerical model is informative in the respect that the validity of the models can be confirmed. The analytical models are informative on how the various parameters influence the result and how they can be adapted to better describe the behavior of the actual physical device, but do not provide the same insight as the analytical models.
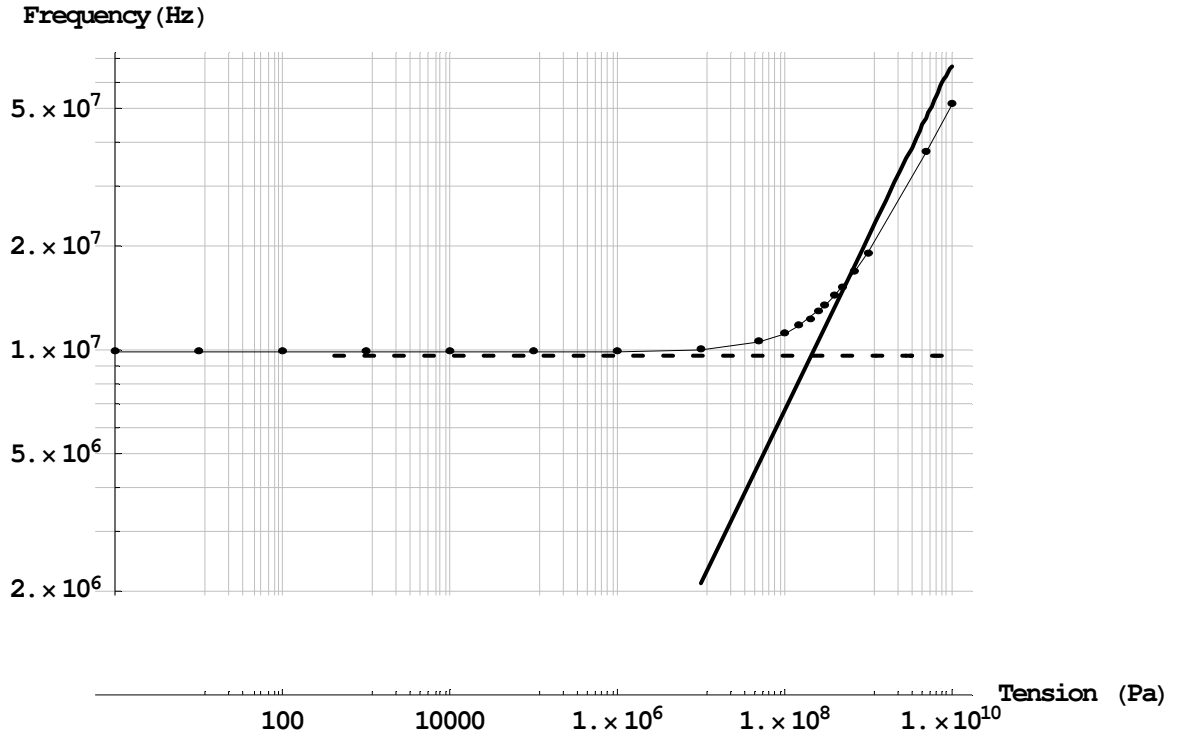

Figure 6.7 Combined resonance frequency results

In figure 6.7 the dashed line is the plot of the plate model at 9.64 MHz. It is a constant, i.e. not stress dependent. The full line is the membrane results where the frequency response has a quadratic response on the intrinsic stress. The dotted line is the numerical result. At low stress levels the numerical model has a higher resonance frequency.

$$f_r = 0.47 \frac{t_{mem}}{a^2} \sqrt{\frac{E}{\rho(1-v^2)}} \tag{7}$$

This is expected because of the stiffening of the membrane by the metallization layer. A doubling of the membrane thickness will also, in the analytic model, double the

frequency. However the decrease in Young's modulus and density of the aluminum will oppose the rise in frequency.

At the high stress range, the numerical and analytical results also are fairly consistent.

$$f_r = 2.4048 \frac{1}{2\pi a} \sqrt{\frac{T}{\rho}} \qquad (9)$$

The behavior of the frequency responses is similar. The analytical result at intrinsic stress of 1 GPa is 21.17 MHz. the corresponding value for numerical model is 19.2 MHz. It is a difference of 9 %. This is also expected since the combined silicon nitride/aluminum membrane has a lower density compared to the analytical pure silicon nitride membrane.

In the transition region where plate and membrane properties give similar results, it evident that the combined effect of plate stiffness and intrinsic stress effects ads up to a higher frequency. This effect, which is displayed in the numerical model, has not been done analytically.

As described in the fabrication part, a membrane made of silicon nitride will have some degree of intrinsic stress. According to the results for resonance frequency modeling it is recommended to tune in the process in to the low stress area. Because of the process variations of LPCVD, the different stress values from each run can be made insignificant. Silicon nitride can be produced with a variation within ±50%. A production process tuned for 30-50 MPa will give predictable specifications of the transducer. If the process is tuned for about 100 MPa or higher it is difficult to foresee the performance of the transducers from run to run.

6.1.7 Collapse voltage

The resonance frequency modeling confirms the dimensions and materials of the transducer. Next step is to model the force possible to apply to the transducer. When increasing the voltage to the electrodes, the membrane will be pulled down. In Comsol Multiphysics modeling the two electrodes are defined as boundary

conditions. The lower surface of the aluminum is defined as the boundary with electrostatic potential. The value is parameterized and named Vin. The top surface of the substrate is defined as the ground plane.
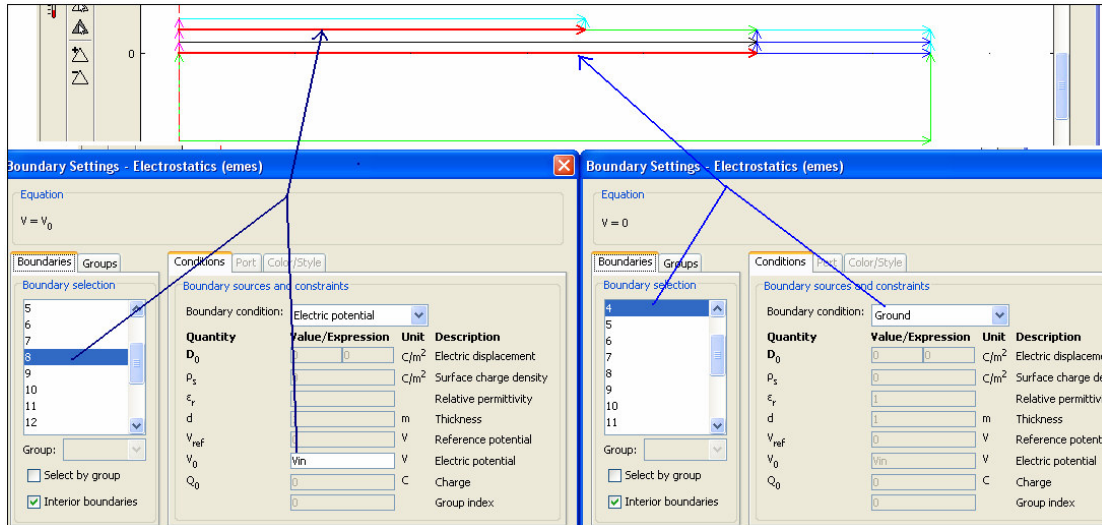

Figure 6.8 Setting electric potential to the model

When applying voltage to the electrodes, the Comsol Multiphysics model will calculate the deflection of the membrane accordingly. When membrane and substrate surfaces cross, the numerical calculations do not make sense and they brake down. In axis-symmetric calculations in Comsol Multiphysics it is not possible define contact pairs to avoid the problem. The way to solve the problem is to set the voltage to high. The log file is then recording the voltage at which the computations failed. This failure voltage is the also defined as the collapse voltage. Finding the collapse voltage has to be done in several runs depending on the accuracy you want. The first run was set to go from1-50 V in steps of 1V. It broke down between 40 and 41 V. Next run is stepping the voltage up to 40 V with steps of 1 V and steps of 0.1 V from 40-41V. The collapse voltage for the structure was found to be 40.7 V.
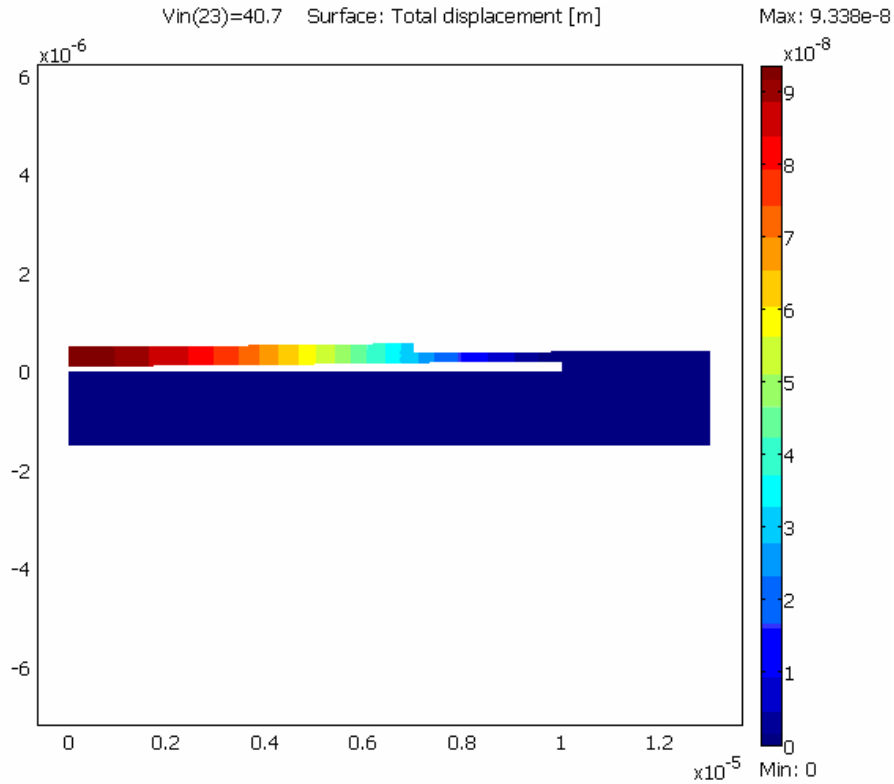
Figure 6.9 Collapse voltage and deflection

The analytic calculations for the collapse voltage do not consider the fact the distance between the electrodes is different over the membrane, but assumes a piston like motion. A numerical model will calculate the curvature of the upper electrode and thereby result in a higher value for the collapse voltage. The analytic calculated collapse voltage is 31V which is 76 % of the numerical calculation. The difference of 9.9V is significant but not unrealistic. The results are in the same order and comparable. According to analytical calculations the electrostatic force at collapse voltage is deflecting the membrane one third of the electrode gap. For a gap of 400nm the deflection should be 133 nm. The numerical analysis indicates a deflection of 93.38 nm at collapse voltage.

6.2   Analytical versus Numerical analysis

The results for the mechanical analysis match quite well. The deviances in results can be explained and are reasonable. The result gives confidence to the models used and the models can be used as a base for further investigations. Even if the results including electrostatics did not mach so well, the results were actually encouraging. The basis for the two models is more different in the electrostatic simulations and thus the results would expect not to match totally. The comparison of the analytical and numerical simulation results gives confidence to conclude that the models are giving correct output and can be used as a base for further work

7 Mask Set Layout

Producing the transducer, several photolithographic steps are involved. One particular mask for each etching or deposition process is required. Naturally, operations including deposition or etching of the entire wafer surface have no need for such a mask. The masks are designed in the L-Edit software, where each layer in the design represents a mask. All fabrication processes are accompanied by process rules. L-Edit has features enabling the user to implement the necessary design rules. Cross checking against the rule setup is possible. Examples of design rules are line width of conductors, spacing between etch cavities etc. The design made for this project is not connected to a specific manufacturer. The design is made on general specification treated earlier in the report.

The wafer bonded cMUT processing has a four mask process. The total mask layout describes one whole element. It is circular with a specified diameter of 2 mm. The whole layout is to be confined into a 2 by 2 mm frame.

7.1 Back side RIE etch

The first process were special features is to be defined is the etching of the cMUT cavities. This is performed on the wafer covered by the Silicon Nitride layer. The cross

section in Figure 7.1 is only a coarse illustration of the cavity set up. The mask is defining the exact lateral dimensions of the cavity. The procedure in L-Edit is to define a layer according mask to be made. The first cavity with the proper dimension is made. In order to fill the whole frame with cavities, the initial cell is duplicated in an array. However, to make the array in an efficient way, the cell is made complete before duplicating.
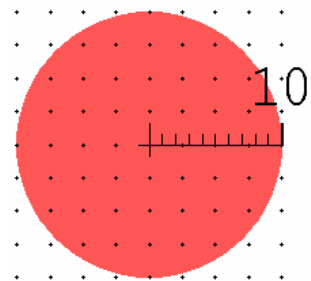
Figure 7.1 Cross section RIE etch

Figure 7.2 One cavity in L-Edit

7.2   Metal conductors

The top electrode is defined on top of the membrane. The process is due at the end of the fabrication line for the transducer. In the mask design it is convenient to deal with the metal layer at this stage. In ch. 4 the general description of the top electrode was decided. 50 % of the cavity area is to be covered. The connecting leads are set to 3 µm width.

One of the most important factors in designing the top electrode is to minimize the electrical resistance. Any reduction of loss is improving the performance of the transducer. For every cell there are six leads in. By making the cross of leads longer than the extent of one cell, all the leads will connect when the cells are set in the final array. Also in this mask the area for the contact pads are defined. Even if the element is 1 mm in radius, it is room for the two necessary contact pads in the corner of the 2x2 mm

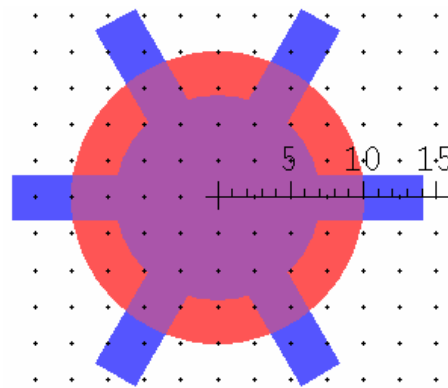**Figure 7.3 Top electrode**

Figure 7.4 L-Edit layout of Aluminum leads

substrate area. In figure 7.3 the removal of the nitride layer on the left hand side of the substrate is shown. The layer for accessing the substrate is described in Ch 7.3.

7.3 Expanding layout to full element size

The finished cMUT cell layout at complete as in figure 7.4. Making the array is done in several steps. First cell is copied to make a row of 100 cells. To insure the membrane support of 0.8 µm, the pitch is set at 20.8 µm. One end cell is moved up to act as the start cell for the second row. In order to get the same pitch in all directions, the displacement of the second row cell is 18 µm in the y-direction. The array is expanded to two full rows. With no
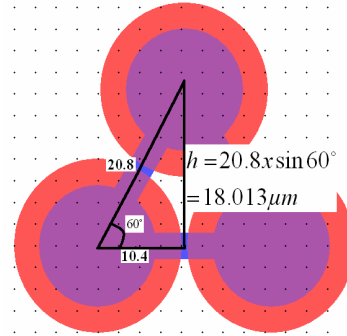

Figure 7.5 Pith calculation for 2nd row

other alignment problems, the full array of 96x96 cells is designed. The design results in a hexagonal pattern of 9220 cell, covering a square of 1.997x1.997 mm. To get the required circular element, all cells extending on or outside a circle with radius of 1 mm are removed. After removing the obsolete cells, about 7450 cells remain. The edge of the element is not uniform because of the orthogonal set up of the cells. All loose aluminum ends of each was connected together to maximize the conductivity.
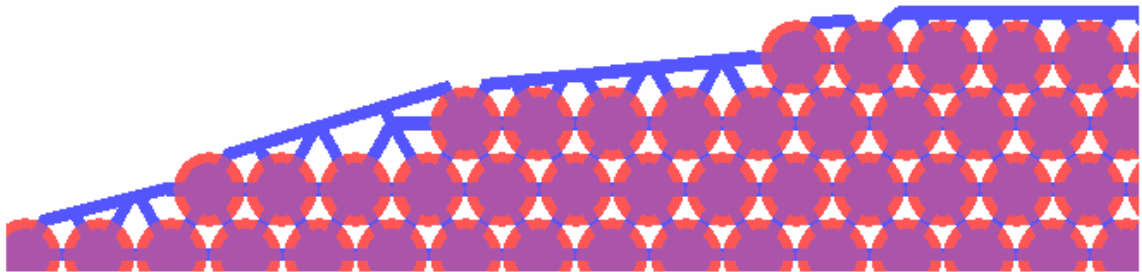

Figure 7.6 Element border irregularities

The last structure to be patterned by the metal layer is the contact pads. The dimensions of the pads are set to 100 x150 µm to ensure a large enough area for the

wire bonder to operate. Another consideration was to make a large contact area to the element in order to get as many cells as possible in direct contact with the contact pad. In figure 7.7 18 rows of cMUTs are connected directly to the contact pad lead.
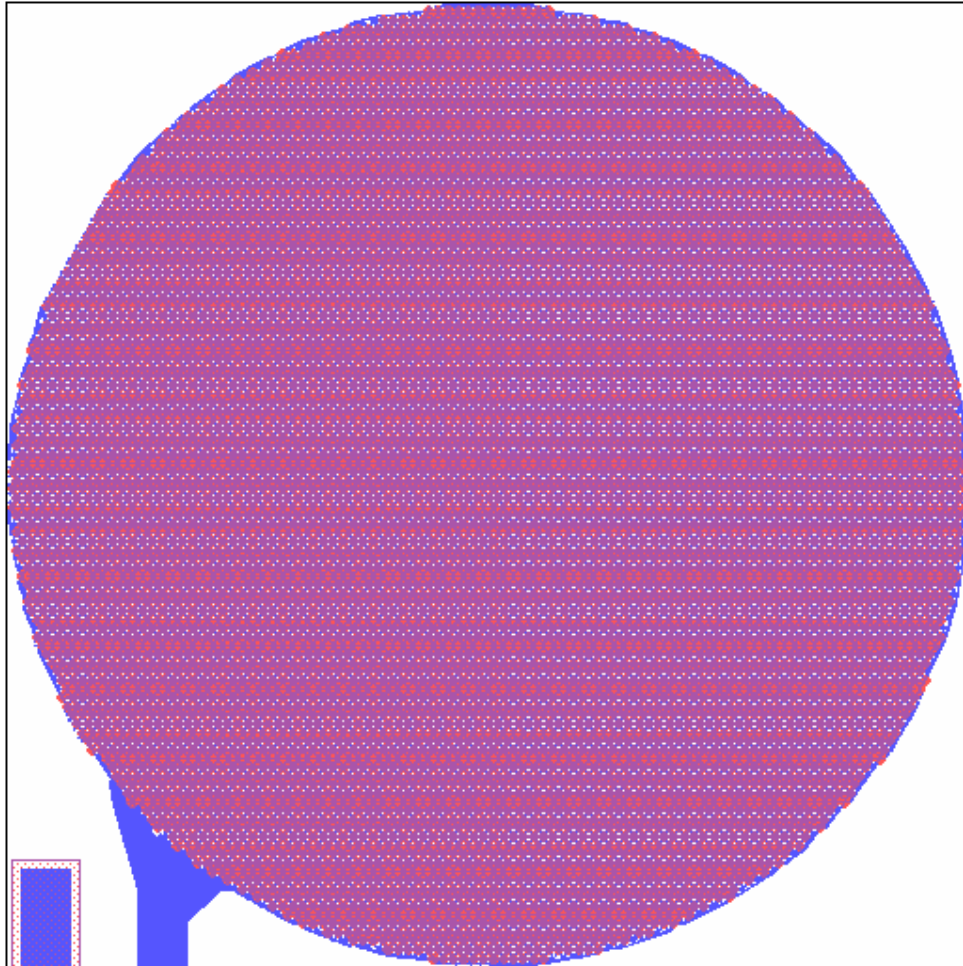

Figure 7.7 Circular element with contact pads

The metal layer is designed in order to minimize the influence on the membrane mechanical properties. To get practical and working contact pads, a second mask is made. Figure 7.8 illustrates the mask for depositing the thick aluminum layer. The layer covers the metal area outside the element area, and ensures proper hold for the bond wire and high electrical admittance.

Figure 7.8 Tick metal mask

7.4   Top side RIE etch

The fourth mask is defining the area on the substrate where the contact pad for the substrate is to be fitted. The Si_3N_4 must be removed in order to exposed the bottom electrode. Both thick and thin aluminum is deposited in this area. Technically for the design of mask layer this is the last layer to design. For the fabrication process, removing the nitride layer has to be done before depositing the metal layers. The nitride "pit" is 30 µm wider in all directions compared with the contact pad. This is just a safety margin to both the depositing and bonding process.
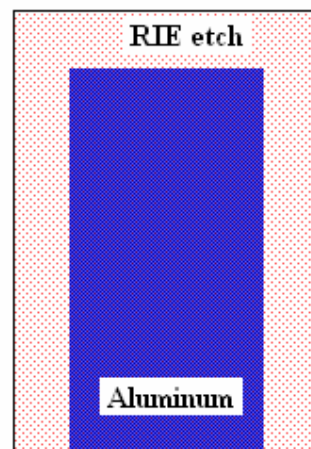

Figure 7.9 RIE etch of Si3N4

7.5   Annular array layout

In order to have a working cMUT transducer, a lot of individual cells must be connected in parallel. The combined area of all the vibrating cells can give a strong enough ultrasound waves to be practical in use. Having more elements connected in the same circuit, the possibility of controlling the direction of the ultrasound wave. Figure 7.10 is an example showing the circular element of 7450 cells divided in four elements with equal area. The result is a four element annular array with approximately 1860 cells in each element. The areas was however divided in four before the trench for the leads were made, resulting in some deviations in the areas. The contact pads for the tree inner areas are placed on the right hand side of the substrate area. The layout is to show the possibilities in the original design. It is not in the scope of the project to design a multielement cMUT.

An annular array allows electronic focusing of the ultrasound beams, in particular, dynamic focusing in reception. This gives a narrower and more constant beam width
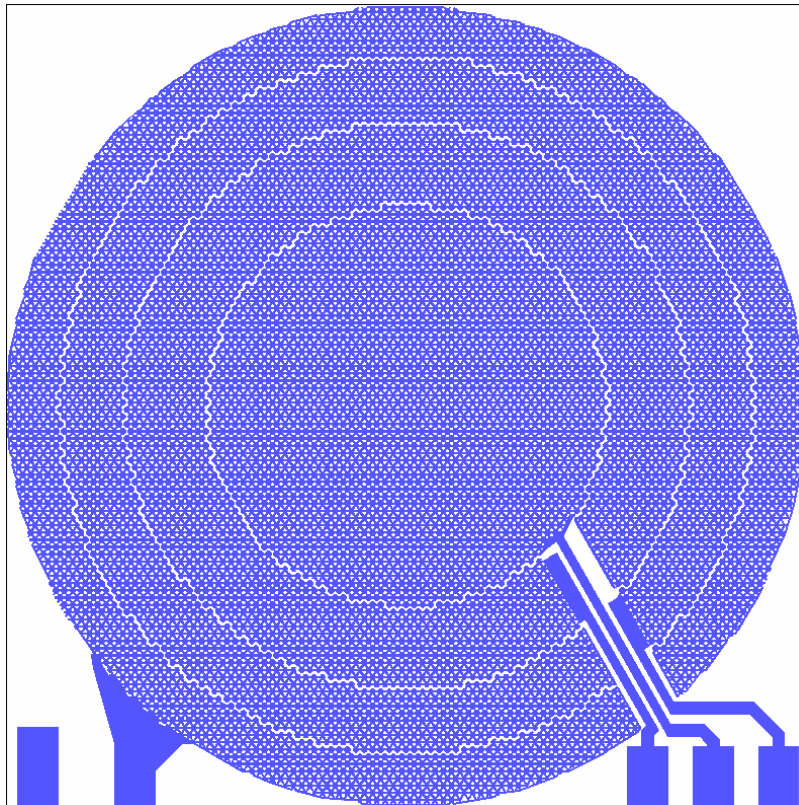

Figure 7.10 Four element annular array

8   Discussions/Further work

The design of a transducer is an extensive task with many aspects to it. Some of them is not being answered too the full in this work. The full analysis of some of the aspects is out of scope of the project. The problems encountered are very relevant for the design and should be addressed in further work on the cMUT.

The use of circular cells in the design is done to better be able to control and compare the different analysis methods. The higher fill factor of a hexagonal cell structure may be an element to consider. A higher fill factor will theoretically improve both emitting and receiving capability of a transducer element. The echo coming from the non active area of the element is also reduced. The amount of improvement is not examined but is important for the final design.

The mask layout is based on a circular element. It may be better, production wise, also to make the element hexagonal. It is possible to dice the wafer in a hexagonal pattern without to much material loss. The total layout also would look better with the same transducer performance.

The task for the project was to design a simple cMUT. A design feature discussed during the work is to change the placing of the contact pads. The contact pads are on the top active side of the element, leaving it challenging to get the wire bonding out of the way of the transducer. One option is to look at trough hole connection to the pads. This will enable the designer to make a package for a forward looking transducer.

The models used in this work are only in the static domain with the DC bias applied. The models used for analytical modeling were modeling two separate situations. One modeled the membrane without any intrinsic stress like a plate model. The second one modeled a membrane without bending stiffness. Making a single model giving the frequency response over the whole range of intrinsic stress levels is however not a trivial task. To analytically get the frequency response where the two separate models cross, it is necessary to develop such a combined model.

Difficulties in getting the first static models verified made it impossible to set aside the time needed for modeling the 10 MHz AC. The next step would have been to apply an AC voltage to model the efficiency of the transducer. The amplitude of the AC signal determines the output pressure from the transducer. For ever device designed for medical applications there are limitations of many kinds. For an ultrasound transducer the pressure output is one. 1 MPa delivered from the transducer

is a limit to be aware of. The trade off between DC- and AC-amplitude, considering both collapse voltage and output pressure, must be modeled.

9   Conclusion

A micromachined ultrasound transducer can be realized with the technologies described in this thesis. Fusion bonding of silicon and silicon nitride has just recently been attempted for producing a capacitive ultrasonic transducer. The research done by Midtbø et al. [1] is most promising. By implementing this technique, durable and insulating membrane of silicon nitride can be utilized in a wafer bonding process. It is shown that the cMUT cavities can be defined with high precision in the membrane material before bonding. In order to uphold a smooth silicon surface for optimal bonding surface, the top electrode is to be diffused into the substrate surface. RIE etch of the nitride layer to form the cavities is an accurate and reproducible process. One of the design conditions was to design the transducer to work at 10 MHz. The design of the transducer is dependent on both material parameters and physical dimensions to meet that condition. Silicon nitride is chosen for membrane and support structure material mainly for two reasons. It is a well known material with excellent membrane qualities. The deposition technologies for the material are well established. Second it is also the chosen material for the research group at NTNU working on the cMUT. The collaboration with the research group will hopefully prove valuable in the future work.

Given the chosen material parameters, analytic models for resonance frequency where used to decide the physical dimensions of the transducer. A membrane with thickness of 200 nm, 20 µm in diameter and a gap of 200 nm meet the requirements quite well. The dimensions are confirmed by the numeric model in Comsol Multiphysics, giving a resonance frequency of 9.93 MHz. The model includes a 200 nm aluminum contact pad covering half the membrane area. It is important to control the intrinsic stress when producing the membrane. The stress must be tuned to around 50 MPa ±50% in order to get a predictable production result.

The bias voltage for the transducer is examined for the transducer dimensions. Standard piston models are used in the analytic modeling, giving a limit of 31 volts before collapse of the membrane. Numerical modeling, which is argued to be closer to a realistic result, is 40.7 volts.

The design is put together into a single element transducer, giving almost 7.500 cells in the element. A mask layout of the transducer element is presented. The descried process only requires 4 mask layers. Finally in the layout a suggestion to divide the element into a array were shown. The array is an annular array with four elements with approximately the same area.

10   Appendix

Table 10.1 Resonance frequency measurements in Comsol Multiphysics

Numerical Comsol Multiphysics-results on resonant frequency at increasing stress. Ch 6.2.4	
Intrinsic stress (Pa)	Resonance frequency (MHz)
1	9,928218
10	9,928218
100	9,928219
10^3	9,928232
10^4	9,928356
10^5	9,929597
10^6	9,942005
10^7	10,065210
5*10^7	10,594870
10^8	11,220630
1.5*10^8	11,812100
2*10^8	12,374280
2.5*10^8	12,911070
3*10^8	12,425560
4*10^8	14,397330
5*10^8	15,305070
7*10^8	16,969760
10^9	19,187430
5*10^9	37,620260
10^10	51,961600

11 Bibliography

[1]   K. Midtbø, K. Schølberg-Henriksen, M. M. V. Taklo, and A. Rønnekleiv, "Surface energy of fusion bonded nitride to silicon", NTNU, Dept of Electronics and Telecommunication, Trondheim, Norway, 2006.

[2]   B. A. J. Angelsen, *Waves, signals and signal processing in medical ultrasonics.* Trondheim: Department of Physiology and Biomedical Engineering, Norwegian University of Science and Technology, 1996.

[3]   U. Demirci, A. S. Ergun, O. Oralkan, M. Karaman, and B. T. Khuri-Yakub, "Forward-viewing CMUT arrays for medical Imaging," *Ieee Transactions on Ultrasonics Ferroelectrics and Frequency Control,* vol. 51, pp. 887-895, Jul 2004.

[4]   D. M. Mills, "Medical imaging with capacitive micromachined ultrasound transducer (cMUT) arrays," General Electric Global Research, Niskayuna, NY, 2004.

[5]   G. Caliano, R. Carotenuto, E. Cianci, V. Foglietti, A. Caronti, A. Lula, and M. Pappalardo, "Design, fabrication and characterization of a capacitive micromachined ultrasonic probe for medical imaging," *IEEE Transactions on Ultrasonics Ferroelectrics and Frequency Control,* vol. 52, pp. 2259-2269, Dec 2005.

[6]   K. Midtbø, P. Storås, and A. Rønnekleiv, "Transfer of silicon nitride to silicon by fusion bonding," NTNU, Dept of Electronics and Telecommunication, Trondheim, Norway, 2005.

[7]   Y. Huang, A. S. Ergun, E. Hæggström, M. h. Badi, and b. T. Khuri-Yakub, "Fabricating Capasitive Micromachined UltrasonicTtransducers With Wafer-Bonding Technology," *Journal of microelectromecanical systems,* vol. 12, pp. 128-137, April 2003.

[8]   X. C. Jin, I. Ladabaum, and B. T. Khuri-Yakub, "The microfabrication of capacitive ultrasonic transducers," *Journal of Microelectromechanical Systems,* vol. 7, pp. 295-302, Sep 1998.

[9]   O. Ahrens, A. Buhrdorf, D. Hohlfeld, L. Tebje, and J. Binder, "Fabrication of gap-optimized cMUT," *Ieee Transactions on Ultrasonics Ferroelectrics and Frequency Control,* vol. 49, pp. 1321-1329, Sep 2002.

[10]   M. Madou, *Fundamentals of microfabrication*. Boca Raton, Fla.: CRC Press, 1997.

[11]   I. Ladabaum, X. C. Jin, H. T. Soh, A. Atalar, and B. T. Khuri-Yakub, "Surface micromachined capacitive ultrasonic transducers," *Ieee Transactions on Ultrasonics Ferroelectrics and Frequency Control,* vol. 45, pp. 678-690, May 1998.

[12]   X. C. Jin, I. Ladabaum, F. L. Degertekin, S. Calmes, and B. T. Khuri-Yakub, "Fabrication and characterization of surface micromachined capacitive ultrasonic immersion transducers," *Journal of Microelectromechanical Systems,* vol. 8, pp. 100-114, Mar 1999.

[13]   A. Lohfink and P. C. Eccardt, "Linear and nonlinear equivalent circuit modeling of CMUTs," *Ieee Transactions on Ultrasonics Ferroelectrics and Frequency Control,* vol. 52, pp. 2163-2172, Dec 2005.

[14]   A. S. Ergun, Y. L. Huang, X. F. Zhuang, O. Oralkan, G. G. Yaralioglu, and B. T. Khuri-Yakub, "Capacitive micromachined ultrasonic transducers: Fabrication technology," *Ieee Transactions on Ultrasonics Ferroelectrics and Frequency Control,* vol. 52, pp. 2242-2258, Dec 2005.

[15]   P. M. Morse and K. U. Ingard, *Theoretical Acoustics*, First Princeton University Press edition ed. Princeton, New Jersey: McGraw-Hill Inc., 1986.

[16]   M.-H. Bao, *Micro mechanical transducers: pressure sensors, accelerometers and gyroscopes*. Amsterdam: Elsevier, 2000.

[17]   A. Nikoozadeh, B. Bayram, G. G.Yaralioglu, and B. T.khuri-Yakub, "Analytical Calculation of Collapse Voltage of CMUT Membrane," *Proceedings of the IEEE Ultrasonics Symposium,* pp. 256-259, 2004.

[18]   R. J. Roark, Young, Warren C., *Roark's formulas for stress and strain*, 6th ed. New York McGraw-Hill,1989.

[19]   S. Olcum, M. N. Selik, C. Bayram, and A. Atalar, "Design Charts to Maximize the Gain-Bandwidth Product of Capacitive Micromachined Ultrasonic Transducers," p. 4.

[20]   W. P. Mason, *Electromechanical transducers and wave filters*. New York: D. Van Nostrand, 1942.